CO adsorption on close-packed transition and noble metal surfaces: trends from *ab initio* calculations

2004 J. Phys.: Condens. Matter 16 1141

(http://iopscience.iop.org/0953-8984/16/8/001)

INSTITUTE OF PHYSICS PUBLISHING JOURNAL OF PHYSICS: CONDENSED MATTER

J. Phys.: Condens. Matter **16** (2004) 1141–1164 PII: S0953-8984(04)73592-4

CO adsorption on close-packed transition and noble metal surfaces: trends from *ab initio* calculations

Marek Gajdoš, Andreas Eichler and Jürgen Hafner

Institut für Materialphysik and Centre for Computational Materials Science, Universität Wien, Sensengasse 8/12, A-1090 Wien, Austria

E-mail: Marek.Gajdos@univie.ac.at

Received 15 December 2003
Published 13 February 2004
Online at stacks.iop.org/JPhysCM/16/1141 (DOI: 10.1088/0953-8984/16/8/001)

Abstract

We have studied the trends in CO adsorption on close-packed metal surfaces: Co, Ni, Cu from the 3d row, Ru, Rh, Pd, Ag from the 4d row and Ir, Pt, Au from the 5d row using density functional theory. In particular, we were concerned with the trends in adsorption energy, geometry, vibrational properties and other parameters derived from the electronic structure of the substrate. The influence of specific changes in our set-up, such as choice of the exchange correlation functional, the choice of pseudopotential, size of the basis set and substrate relaxation, has been carefully evaluated. We found that, while the geometrical and vibrational properties of the adsorbate–substrate complex are calculated with high accuracy, the adsorption energies calculated with the gradient-corrected Perdew–Wang exchange–correlation energies are overestimated. In addition, the calculations tend to favour adsorption sites with higher coordination, resulting in the prediction of the wrong adsorption sites for the Rh, Pt and Cu surfaces (hollow instead of top). The revised Perdew–Burke–Erzernhof functional (RPBE) leads to lower (i.e. more realistic) adsorption energies for transition metals, but to the wrong results for noble metals—for Ag and Au, endothermic adsorption is predicted. The site preference remains the same. We discuss trends in relation to the electronic structure of the substrate across the periodic table, summarizing the state-of-the-art of CO adsorption on close-packed metal surfaces.

1. Introduction

The development of modern theoretical surface science provides an opportunity to investigate surfaces and adsorbate structures on the atomic scale with useful applications in industrial technologies. Much effort has been devoted to studying CO chemisorption and dissociation on transition metals. There are numerous papers and reviews which deal with this system from different points of view (electronic, structural, vibrational) [1–4]. One of the central questions is how the strength of the chemisorption of CO and the preference for the specific adsorption

site varies across the transition metal (TM) series. A particular case, CO adsorption on the Pt(111) surface, has attracted much attention in the past, since for this system state-of-the-art DFT calculations fail in predicting the correct site preference [5]. The question which immediately arises is whether this case is an exception or the rule.

In addition, a vast number of theoretical papers have appeared in the literature since Ying *et al* [6] presented in the mid-1970s a first self-consistent density functional study of chemisorption on metal surfaces (H on tungsten). The number of theoretical adsorption studies of TM molecules on different surfaces is increasing with time, not only because of their importance in catalysis, but also due to the increasing reliability of the 'measured' properties. In the past, several systematic studies of the adsorption of CO molecules on transition metal surfaces have been performed [2, 7–9]. In 1990 Nørskov [8, 9] proposed a model of chemisorption on transition metal surfaces which was later expanded and is now quite generally accepted. A main feature of the model is the importance of the position of the d-band centre relative to the HOMO and LUMO of the adsorbate. The importance of understanding the correlation between the geometric and the electronic structure arises from the proposed mechanistic model for chemisorption. One among several trends is the correlation between the CO stretching frequency ν_{C-O} and the energy level difference between 5σ and 1π orbitals of the adsorbed CO ($\Delta(5\tilde{\sigma} - 1\tilde{\pi})$) proposed by Ishi *et al* [10].

In this paper we present an extensive density functional study of the adsorption of CO on the close-packed surfaces ((111) for face-centred cubic, resp. (0001) for hexagonal metals) of Co, Ni, Cu, Ru, Rh, Pd, Ag, Ir, Pt and Au. After a description of the set-up in section 2, we characterize briefly the clean surfaces in section 3. Section 4 is devoted to the adsorption of CO. Starting from the geometric structure of the adsorbate–substrate system, going through the vibrational and electronic properties (stretching frequencies of the adsorbate, and of the adsorbate–substrate bond, occupation of the anti-bonding $2\pi^\star$-like orbital, density of states and redistribution of the charge density) as well as the site preference we draw a complete picture of the CO adsorption on the close-packed TM and noble metal surfaces. Moreover, we investigate the influence of the exchange–correlation functional and the cut-off energy on the site preference (section 5). In section 6 we discuss our results in the light of the experimental literature and analyse trends and correlations between the properties investigated. This paper tries to go beyond a pure table of references from experiments and different DFT calculations by providing a large and consistent database, in which each element was treated in exactly the same manner. Further, one of our main goals is not only to obtain theoretical values of spectroscopic accuracy, but also to derive useful trends of CO adsorption on 3d, 4d and 5d transition metal surfaces with the hope of applicability in the prediction of the adsorption and catalytic behaviour.

2. Methodology

The calculations in this work are performed using the Vienna *ab initio* simulation package VASP [11, 12] which is a DFT code, working in a plane-wave basis set. The electron–ion interaction is described using the projector-augmented-wave (PAW) method [13, 14] with plane waves up to an energy of $E_{cut} = 450$ eV (for some calculations, harder pseudopotentials were used for C and O which require an energy cut-off of 700 eV). For exchange and correlation the functional proposed by Perdew and Zunger [15] is used, adding (semi-local) generalized gradient corrections (GGA) of various flavours (PW91 [16], RPBE [17]). These GGAs represent a great improvement over the local density approximation (LDA) in the description of the adsorption process.

The substrate is modelled by four layers of metal separated by a vacuum layer of approximately double thickness, as shown in figure 1. The two uppermost substrate layers and

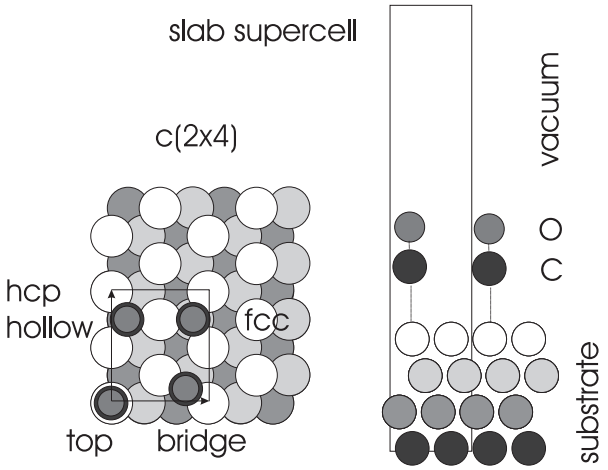

Figure 1. Top and side view of the slab used in the calculations. In the top view of the c(2 × 4) cell we show all investigated high-symmetry sites.

the CO molecule are allowed to relax. This enables us to check the influence of the relaxation on the adsorption system. The Brillouin zone of the c(2 × 4) surface cell (equivalent to a coverage of $\Theta = 0.25$ ML) was sampled by a grid of (4 × 3 × 1) k points. We have chosen this coverage as a compromise between small adsorbate–adsorbate interactions ('low coverage limit') and low computational effort.

In the calculation we investigated the adsorption on the close-packed surfaces of 10 metallic elements from the 3d (Co, Ni, Cu), 4d (Ru, Rh, Pd, Ag) and 5d (Ir, Pt, Au) transition metal rows of the periodic table. For all hcp elements, Co and Ru, the (0001) surface was used with the ideal c/a ratio of 1.63. The spin polarization of Ni and Co was also taken into account.

Vibrational properties of CO were computed by applying a finite-differences method to create the Hessian matrix which we diagonalize to obtain the characteristic frequencies. We have calculated the metal–CO (ν_{M-CO}) and C–O stretching (ν_{C-O}) frequencies in the direction perpendicular to the surface plane.

The free CO molecule is characterized by a calculated stretching frequency of 2136 cm^{-1} at an equilibrium bond length of 1.142 Å. The corresponding experimental values are 2145 cm^{-1} and 1.128 Å [18]. The problem of too large a CO binding energy ($E_{CO}^{PW91} = 11.76$ eV, $E_{CO}^{exp} = 11.45$ eV [19]) stems mainly from the error in the energy of the free atom, where high density gradients make an accurate description more difficult.

Further, the bonding of an adsorbate to the surface by calculating the density of states and charge density flow was investigated.

3. Bulk and clean surfaces

3.1. Lattice constant

For a general understanding of the adsorption process, especially for the adsorption in higher coordinated sites, the lattice constant of the substrate is an important parameter. The optimal adsorption height, for example, will always be determined by an interplay between the optimal carbon–metal bond length and the lattice parameter. For that reason, we give in figure 2

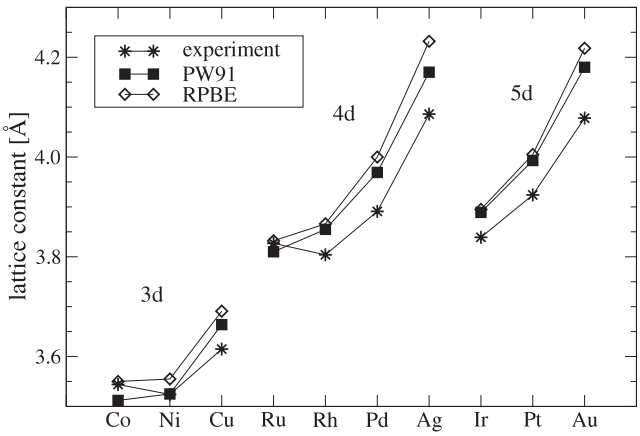

Figure 2. Lattice parameters for a part of the periodic table. We show the experimental and calculated lattice parameters for the PW91 and RPBE functionals. Although Ru and Co are hcp metals we have included them, together with fcc metals, at an ideal $c/a \doteq 1.63$.

the theoretical lattice constants together with the experimental values [20]. These lattice parameters are compared with lattice parameters calculated with the PW91 and RPBE exchange correlation functional.

The overestimation of the lattice parameter (calculated within the GGA) is characteristic for the heavier elements. The difference between the experimental and calculated lattice constant is around 1% for 3d row metals and around 2% for the other elements. Such a 2% difference in the lattice constant corresponds to a change in the CO adsorption energy of about 0.03 eV for Pd(100) [21] and Ru(0001) surfaces [22]. In general, the lattice parameter increases along the rows and columns of the periodic table. For a larger lattice constant one might expect that the adsorbate will come closer to the surface. On the other hand, as the width of the d band increases, the binding is reduced and the actual height of the adsorbate over the surface should increase.

3.2. Work function

In figure 3 we present the calculated work functions together with experimental values.

We find that the calculated work functions (PW91) are, in all cases, slightly lower (by at most 6% for Ag) than the measured values. The largest discrepancies in terms of absolute values are found for 4d metals, where the differences for the Ru, Rh and Ag surfaces are $\approx$0.3 eV. However, in general the agreement is quite good. The work function always increases with the d-band filling. Only for the noble metals (Cu, Ag, Au) does it decrease again. Similarly, the work function increases along the columns when going down from the 3d to the 5d metals.

3.3. Electronic structure: d-band centre

The position of the d-band centre of the clean surface is another important characteristic which is closely related to the strength of the CO–surface interaction. As was already argued [8, 29, 30], the d-band centres play a significant role in the bonding for many adsorbate–substrate systems where the major interaction is due to hybridization of the HOMO and LUMO of the adsorbate and the d orbitals of the substrate.

However, simple as it might seen to be, the proper definition of the d-band centre is not that straightforward:

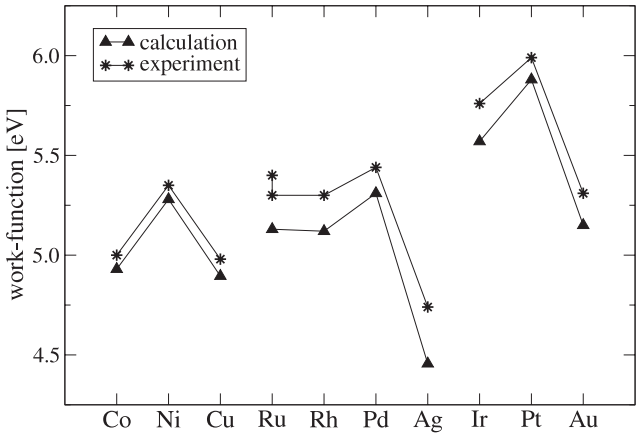

Figure 3. Experimental and calculated values of the work function (PW91) for various transition metal (111) surfaces. References for the experiments: Co [23], Ni [23], Cu [23], Ru [24, 25], Rh [26], Pd [27], Ag [23], Ir [23], Pt [26, 28], Au [23].

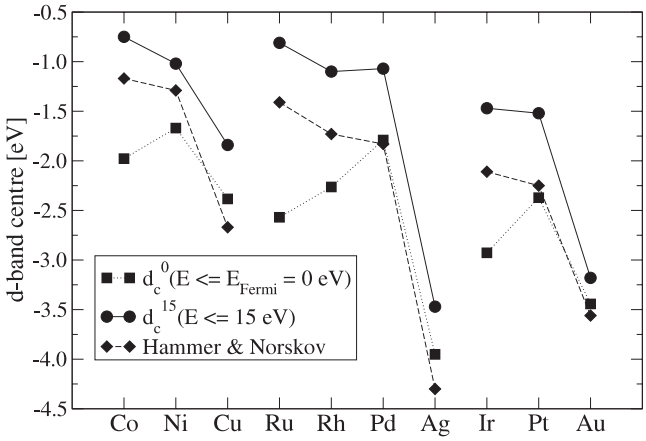

Figure 4. The d-band centres of the clean TM surfaces integrated until the E_{Fermi} level and 15 eV above E_{Fermi}, where at least 9.5 electrons are accommodated in the d band. As a comparison the calculated d-band centres from the paper of Hammer and Nørskov are shown [8].

(i) Within a plane-wave method, partial angular-momentum decomposed densities of states can be defined in different ways. We choose the projection of the plane-wave components onto spherical orbitals within some atomic radius.

(ii) DFT applies only to the ground state; excited states are usually predicted at too low energies. Therefore we report in figure 4 the centre of gravity of the occupied d-band (integration up to the Fermi level) d_{c}^{0} and the centre of the entire d-band d_{c}^{15} (integration from the lower band edge up to 15 eV above E_{Fermi} where at least 9.5 electrons have been accommodated in the d band), together with the d-band centres taken from the older LMTO calculations of Hammer and Nørskov ($d_{\mathrm{c}}^{\mathrm{HN}}$) [8]. The d_{c}^{0} and d_{c}^{15} values provide upper and lower bounds for our d-band centres. The $d_{\mathrm{c}}^{\mathrm{HN}}$ lies in between for TM surfaces, but it is lower in energy for noble metals. This stems from a small contribution to the density of states far from the main d-band peak. As per definition, the difference between

d_c^0 and d_c^{15} increases with decreasing band filling. d_c^{15} shows only a little variation in groups VIII to IB. As expected, it drops significantly for the noble metals compared to metals in the same row.

4. CO adsorption

We have studied the adsorption of CO in the top, bridge and hollow (fcc, hcp) sites in the c(2 × 4) cell, corresponding to a coverage of a quarter of a monolayer ($\Theta = 0.25$ ML) (see figure 1). From these calculations we derive in the following trends in the adsorption energies, the vibrational properties, the geometric and the electronic structure.

4.1. Adsorption energy and site preference

Besides the adsorption geometry and the vibrational properties a precise determination of the adsorption energy for a given geometry is one of the keys to understanding the mechanism of catalytical activity and selectivity [31]. The adsorption energy describes the strength of the chemical bond between the CO molecule and the metallic surface.

The adsorption energy for the stable adsorption site corresponds to the absolute minimum on the potential energy surface (PES) of the molecule moving on the surface. The adsorption energies calculated for other high-symmetry sites correspond either to local extremes or to a saddle point on the PES. The position and height of the saddle points define the diffusion path and the activation energy for surface diffusion.

The experimental isosteric heat of the adsorption $H_{ads}(\Theta)$ is not directly comparable with the calculated adsorption energy. If we want to compare our theoretically calculated adsorption energy E_{ads} (i.e. the gain in energy when a certain amount of CO is adsorbed) at $\Theta = 0.25$ ML with the isosteric heat of adsorption (a differential energy gained when adsorbing one additional molecule on a surface at a certain CO coverage) we need to take the integral up to the coverage used in the calculation:

$$H_{ads,int}(\Theta_{calc}) = \frac{1}{\Theta_{calc}} \int_0^{\Theta_{calc}} H_{ads}(\Theta)\, d\Theta. \tag{1}$$

The experimental heats of adsorption and the proposed adsorption sites are presented in table 1. We show adsorption sites which are found at 0.25 ML or up to 0.5 ML coverage.

The main trends in the experimental results given in table 1 include:

(i) CO adsorption on TM surfaces is several times stronger ($E_{ads} \sim 1.2$–1.7 eV) than on noble metals ($E_{ads} \sim 0.3$–0.5 eV).
(ii) All measured adsorption sites (with the exception of the on-top site on Ru(0001)) show a slight decrease of the heat of adsorption going from the zero coverage limit to a quarter-monolayer coverage.
(iii) The heat of adsorption decreases with increasing filling of the d band.

Figure 5 summarizes the calculated adsorption energies (using the PW91 GGA) for the high symmetry positions described in figure 1. For the transition metals we note a pronounced tendency to overestimate the adsorption energies—this is independent of an eventual relaxation of the surface. For the noble metals (with the exception of Cu), on the other hand, the calculations rather tend to underestimate the adsorption energies—this could be related to the neglect of dispersion forces.

Experimentally, the adsorption energies on the TM surfaces are found to decrease monotonically with increasing band filling. In the calculation, the variation depends on

Table 1. Experimental heats of adsorption for $\Theta = 0$ and 0.25 ML (if available) and the integral heat of adsorption between the zero limit and 0.25 ML. Integral heats of adsorption $H_{ads,int}$ are compared with our calculated adsorption energies E_{ads} at the experimentally observed adsorption sites for the PW91 and RPBE exchange–correlation functionals using two different sets of pseudopotentials ($E_{cut} = 450, 700$ eV, cf the text). TDS—thermal desorption spectroscopy, CAL—calorimetry method, He—helium scattering method, LITD—light-induced thermal desorption, SP–SP measurement, TREELS—time resolved electron energy loss spectroscopy.

		Experiment						Theory		
Surface	Site	H_{ads} (0 ML)	H_{ads} ($\frac{1}{4}$ ML)	$H_{ads,int}$	Method	Θ (ML)	Ref.	$E_{ads}^{PW91,450}$	$E_{ads}^{PW91,700}$	$E_{ads}^{RPBE,700}$
Co	Top	−1.33	−1.33	−1.33	SP	0.33	[32]	−1.65	−1.62	−1.32
		−1.19			TDS		[33]			
Ni	Hollow	−1.35	−1.28	−1.32	CAL	0.25	[34]	−1.95	−1.90	−1.44
		−1.31	−1.28	−1.30	TDS	0.25	[35]			
		−1.31	−1.06		TDS	0.25	[36]			
Cu	Top	−0.49			TDS		[37]	−0.75	−0.72	−0.42
		−0.425			TDS		[38]			
		−0.46			TDS	0.33	[39]			
Ru	Top	−1.66	−1.66	−1.66	TDS	0.20	[40]	−1.89	−1.82	−1.69
Rh	Top	−1.5	−1.38	≈−1.44	TDS	0.2–0.25	[41]	−1.89	−1.86	−1.55
		−1.37	−0.77	≈−1.07	TDS	0.25	[42]			
		−1.71			TREELS		[43]			
		−1.40	−1.28	−1.36	He		[44]			
Pd	Hollow	−1.30			TDS		[45]	−2.14	−2.09	−1.68
		−1.54	−1.30	≈−1.42	TDS	0.25	[46]			
Ag	Top		−0.28		TDS		[47]	−0.16	−0.14	0.18
Ir	Top	−1.81	−1.55	≈−1.63	TDS	0.25	[48]	−1.98	−1.94	−1.64
			−1.52			0.33	[49]			
Pt	Top	−1.50			TDS	0.25	[50]	−1.70	−1.67	−1.34
		−1.39	−1.22	≈−1.33	LITD	0.25	[51]			
		−1.43	−1.30	≈−1.37	TDS	0.25	[52]			
Au	Top		−0.40		TDS		[53]	−0.32	−0.24	0.12

the adsorption site: E_{ads} decreases for on-top adsorption but increases for sites with higher coordination. This leads to the wrong predictions for Cu, Rh and Pt, where the hollow sites were found to be preferred for CO adsorption, whereas experiment shows that adsorption occurs on the top sites. Moreover, the relaxation of the metallic substrate is necessary for Co and Ru surfaces and a denser k-point ($8 \times 6 \times 1$) is required for all surfaces, i.e. if the surface is not allowed to relax (or k-point convergence is not achieved) we get a different site prediction compared to experiment. However, even after substrate relaxation, the energies for CO adsorption in hollow and top sites on Co, Ag and Au surfaces remain almost degenerate. Site preference is indeed a fundamental problem for CO adsorption on metallic surfaces. We shall try to elucidate the origin of this problem below.

Another interesting point is that, among the hollow sites, the preference changes from hcp (Co, Ni, Ru, Rh, Ir) to fcc (Cu, Pd, Ag, Pt, Au) with increasing d-band filling.

4.2. Geometric structure

In the past many studies have demonstrated that, on the basis of DFT, a reliable determination of the geometrical structure is possible. The local adsorption geometry of the CO molecule on

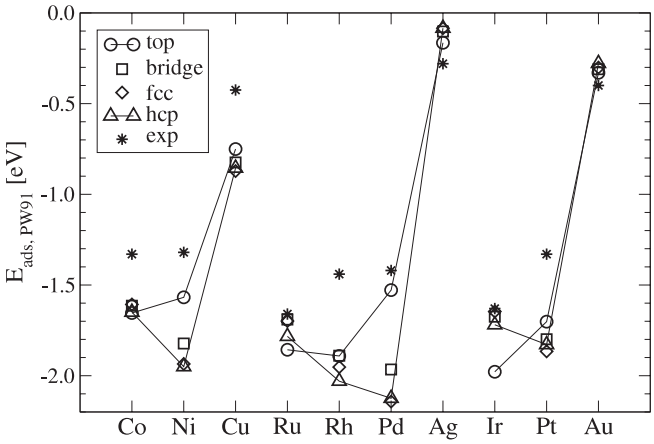

Figure 5. Calculated CO adsorption energies on TM surfaces for the PW91 exchange–correlation functional and an energy cut-off of 450 eV. Experimental CO heats of desorption are labelled by the stars (see table 1).

an unrelaxed TM surface can uniquely be characterized by the S(surface)–C distance (height above the surface) and the C–O bond length. If additionally the metal atoms are allowed to relax, this modification of the surface can be described by the change of the inter-layer distance and the buckling of the surface.

On all studied surfaces the CO molecule adsorbs in an upright position with the carbon atom pointing towards the surface. The tilt with respect to the surface normal is always less than 2°.

The minimum distance between neighbouring adsorbates varies in our set-up (c(2 × 4)) between 4.3 Å (Co) and 5.1 Å (Au). Therefore direct as well as indirect interactions can be considered to be small and our calculations probe the low-coverage case.

In response to the adsorption of the CO molecule, the metal atoms in the immediate surroundings move outwards. This effect is quite localized. The buckling is less pronounced for adsorption in higher coordinated sites (∼0.1 Å) and increases for one-fold-coordinated CO in an on-top position to ∼0.2 Å.

The height of the CO molecule above the surface (d_{S-C}) is determined by the extension of the metal d orbitals and (for the higher coordinated sites) by the nearest-neighbour distance of the substrate atoms. The greater the extension of the interacting metal orbitals the larger is the distance between the C atom and the closest metal atom (d_{M-C}). Similarly, for a given metal–C distance, the molecule will adsorb at a lower height for greater lattice constants. The essential importance of the metal–carbon bond distances for understanding the mechanism of the metal–CO bonding was pointed out earlier [10].

As was already indicated in the previous studies, a different occupation of the interacting d-band orbitals leads to different values for the d_{S-C} and d_{M-C} lengths. In figures 6 and 7 the main characteristics of the CO adsorption geometry on TM surfaces are compiled.

When comparing the adsorption geometry, the noble metals behave differently from all other metals. This reflects the completely filled d band and hence the different bonding mechanism. Adsorption on the noble metals is significantly weaker (see adsorption energies, figure 5), and consequently the d_{S-C} and d_{M-C} lengths are enhanced (see figure 6). On the other hand, CO adsorption on the surfaces of TM is stronger and d_{S-C} (resp. d_{M-C}) tends to decrease as the filling of the d band increases. This trend is more pronounced for 4d than for 5d or 3d metals (for Co and Ni this does not hold for on-top adsorption). For on-top adsorption,

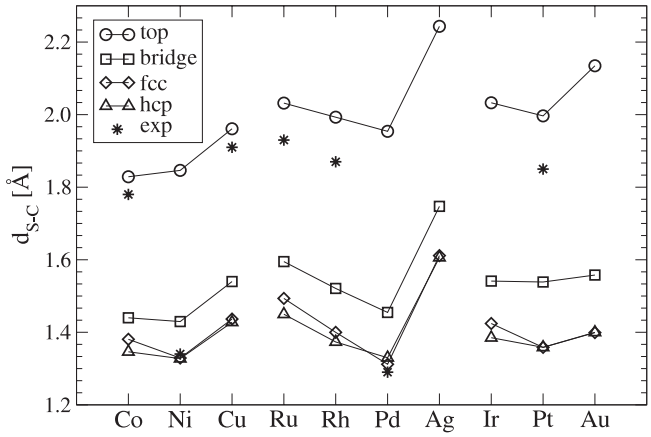

Figure 6. Calculated heights of the CO adsorbate (surface–C distance) in different adsorption sites on various TM surfaces together with values taken from the experimental literature (table 2).

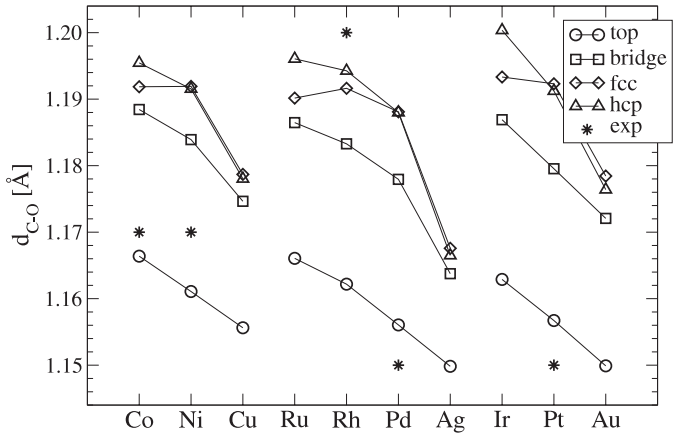

Figure 7. Calculated C–O bond lengths in top, bridge, fcc and hcp hollow sites on TM surfaces together with experimental values as listed in table 2.

the height of the adsorbate increases going from 3d via 4d to 5d elements. The coordination has a strong effect on the CO height: CO in the lower coordinated sites is closer to the surface.

The C–O bond length (d_{C-O}) of the free molecule was calculated to be 1.142 Å. On adsorption, the d_{C-O} length increases with the coordination of the adsorption site, similarly to d_{S-C} and d_{M-C}: d_{C-O} increases from 1.15–1.17 Å for one-fold- to 1.17–1.20 Å for three-fold-coordinated sites. This trend was already stressed in the experimental work of Westerlund *et al* [54]. In addition, the C–O bond is more elongated as the filling of the d band decreases.

There are many data for the geometrical structure of the CO adsorption on TM from past experiments [55–62]. Only for iridium, gold and silver surfaces are we not aware of any experimental literature. A valuable collection of detailed experimental data for the adsorption of small molecules on metallic surfaces can be found in the study of Over [3]. A part of the vast data is presented in table 2.

The main difficulty in comparison with experiment (LEED, XPD, EXAFS, etc) is that the estimated error for the C–O bond length ($\sim\pm0.05$ Å) is mostly too large, covering the

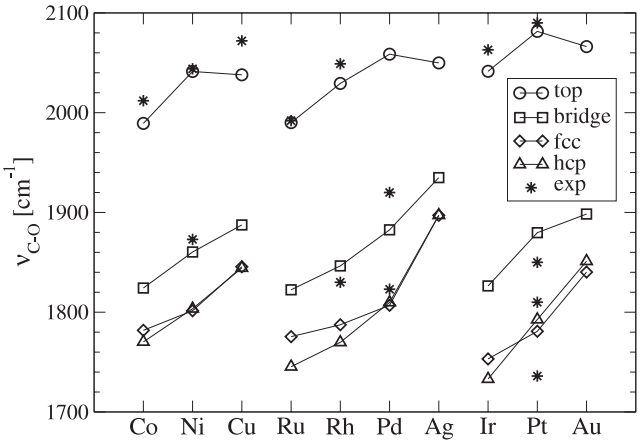

Figure 8. Calculated C–O stretching frequencies (ν_{C-O}) on close-packed TM surfaces together with experimental values as listed in table 3. The calculated value of ν_{C-O} for the free CO molecule is 2136 cm^{-1} compared to the experimental value of 2145 cm^{-1}.

Table 2. Experimental geometrical structures from low energy electron diffraction (LEED) studies of the CO adsorption on TM surfaces together with the values obtained in this study (superscript 'cal'). The normal distance between carbon and the TM surface (d_{S-C}) and the C–O bond length (d_{C-O}) at a coverage Θ are shown together with corresponding references.

		Experiment				Theory	
Surface	Site	d_{S-C} (Å)	d_{C-O} (Å)	Θ (ML)	Ref.	d^{cal}_{S-C} (Å)	d^{cal}_{C-O} (Å)
Co	Top	1.78 ± 0.06	1.17 ± 0.06	0.33	[55]	1.83	1.166
Ni	Hollow	1.34 ± 0.07	1.15 ± 0.07	0.5	[56]	1.329	1.192
	Hollow	1.29 ± 0.08	1.18 ± 0.07	0.5	[56]	1.327	1.192
Cu	Top	1.91 ± 0.01		0.33, 0.44	[57]	1.96	1.156
Ru	Top	1.93 ± 0.04	1.10 ± 0.05	0.33	[58]	2.03	1.166
Rh	Top	1.87 ± 0.04	1.20 ± 0.05	0.33	[59]	1.99	1.162
Pd	Hollow	1.27 ± 0.04	$1.14^{+0.14}_{-0.11}$	0.33	[60]	1.31	1.188
	Hollow	1.29 ± 0.05	1.15 ± 0.04	0.33	[61]	1.33	1.188
Pt	Top	1.85 ± 0.10	1.15 ± 0.1	0.3	[62]	2.00	1.157

whole interval of all calculated d_{C-O} values. Although the c(2 × 4)–CO structure used in the calculation is not realized on all metallic surfaces, values for p($\sqrt{3} \times \sqrt{3}$) and p(2 × 2) structures give values in line with our results. This implies that the CO adsorbate–adsorbate interactions at a coverage lower than $\Theta = \frac{1}{3}$ ML play only a minor role.

4.3. Vibrational frequencies

Vibrational frequencies can be measured very accurately using infrared spectroscopy (RAIRS), electron energy loss spectroscopy (EELS) and sum frequency generation (SFG) methods. The dependence of the stretching frequency ν_{C-O} on the coordination by the surface atoms has often been used as an indication of the adsorption site. The correlation between the vibrational and electronic properties was analysed in the paper by Ishi *et al* [10] in which a correlation between ν_{C-O} and the energy level difference between the $5\tilde{\sigma}$ (5σ character after adsorption) and $1\tilde{\pi}$ orbitals of the adsorbed CO ($\Delta(5\tilde{\sigma} - 1\tilde{\pi})$) was suggested.

In the following we will focus on two eigenmodes: the M–CO (ν_{M-CO}) and the C–O (ν_{C-O}) stretching frequencies. Our calculated ν_{C-O} values are compiled in figure 8. For free

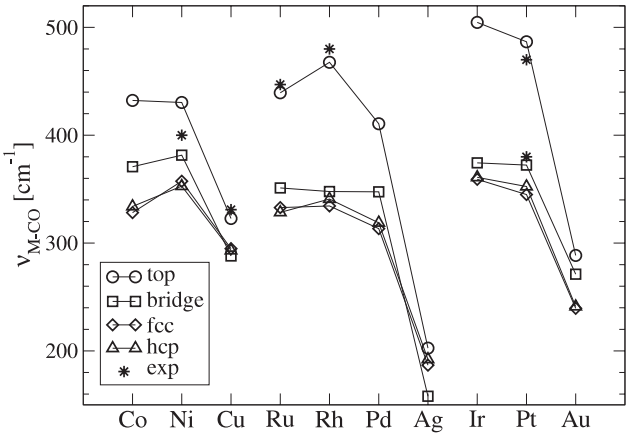

Figure 9. Calculated M–CO vibrational frequencies (ν_{M-CO}) on close-packed TM surfaces together with experimental values as compiled in table 3.

CO molecules a stretching frequency of $\nu_{C-O} = 2136$ cm^{-1} was calculated. This value is lowered due to the formation of the bond between the molecule and the metallic surface. The C–O vibrations exhibit the expected strong coordination dependence: CO molecules adsorbed in the lower coordinated sites vibrate faster and typical values for the C–O stretching frequency are 1990–2100, 1830–1880 and 1750–1810 cm^{-1} for CO in the top, bridge and hollow sites, respectively. The stretching frequency for the CO molecule in bridge and hollow sites on noble metals is higher than on the TM whereas for on-top adsorption the frequencies are almost the same for the noble metals and those of the Pt group.

The dependence of ν_{C-O} on the d-band filling of the substrate is also obvious: increased d-band filling raises ν_{C-O}; the correlation is essentially linear. An exception to the rule is CO in on-top sites on noble metals. With decreasing d-band filling the stretching frequencies for the CO adsorbed in the fcc and hcp hollows begin to differ, with the lower ν_{C-O} for the hcp sites.

The adsorbate–substrate stretching frequencies ν_{M-CO} are compiled in figure 9. ν_{M-CO} exhibits a similar coordination dependence as ν_{C-O}: CO molecules adsorbed in the lower coordinated sites vibrate faster, typical intervals of the ν_{M-CO} stretching frequencies on the TM surfaces being 400–475, 340–380 and 300–350 cm^{-1} for the top, bridge and hollow sites, respectively. There is no pronounced correlation with the d-band filling. For noble metals ν_{M-CO} lies generally below 300 cm^{-1} and there is only a very weak site dependence. Once more, this reflects the weak CO–noble metal bonding. The metal–substrate stretching frequency is particularly low for the Ag surface, consistent with a very low adsorption energy. We have collected the available experimental data for ν_{C-O} and ν_{M-CO} frequencies in table 3 and included them in figures 8 and 9. Agreement between experiment and theory is very good.

As a final remark we emphasize that here only high symmetry sites have been considered. A mixed occupation of different sites or off-symmetry adsorption at higher coverages can significantly increase the CO stretching frequency. As an example we refer to a recent publication on adsorption of CO on the Ni(111) surface presented by Eichler [56].

4.4. Electronic structure

The electronic structure provides a deep insight into the interaction between adsorbate and surface. There are many papers which deal with electronic structures and their influence

Table 3. Experimental and calculated metal–CO (ν_{M-CO}) and C–O vibrational frequencies (ν_{C-O}) of CO adsorbed on 3d and 4d TM surfaces. The coverage Θ and references to the experimental studies are added. RAIRS—reflection-absorption infra-red spectroscopy, (HR)EELS—(high resolution) electron energy loss spectra, SFG—sum frequency generation spectroscopy.

		Experiment					Theory	
Surface	Site	ν_{M-CO} (cm^{-1})	ν_{C-O} (cm^{-1})	Θ (ML)	Method	Ref.	ν^{cal}_{M-CO}	ν^{cal}_{C-O}
Co	Top		2012	0.33	RAIRS	[63]	432	1989
Ni	Top		2044	0.25	RAIRS, HREELS	[56]	430	2041
	Hollow	400	1873	0.25	RAIRS, HREELS	[56]	353	1804
Cu	Top	346	2072		RAIRS	[64]	323	2038
		331	2077	0.33	EELS, RAIRS	[65]	—	—
			2075	Low (0.5 L)	RAIRS	[66]	—	—
Ru	Top	445	1980–2080	0.07	EELS	[67]	439	1990
		447	1990	0.33	RAIRS	[68]	—	—
			1992	0.25	HREELS	[69]	—	–
Rh	Top		2000	0.33	HREELS	[59]	468	2029
		480	1990	Low	HREELS	[70]	—	—
			2049	0.2	HREELS	[71]	—	—
	Hollow		1830	0.2	HREELS	[71]	328	1782
Pd	Hollow		1848	0.33	RAIRS	[60]	319	1810
			1823	<0.25	RAIRS	[72]	—	—
			1823–1850	<0.33	HREELS	[73]	—	—
	Bridge		1920	0.5	RAIRS	[60]	348	1883
Ag	Top		2137	Low (2 L)	HREELS	[74]	203	2050
Ir	Top		2063	Low (1 L)	RAIRS	[48]	505	2041
			2028–2090	0–0.71	RAIRS	[75]	—	—
			2065	0.25	RAIRS	[76]	—	—
Pt	Top	470	2100	0.24	EELS	[50]	487	2081
			2090		SFG	[77]	—	—
		464		0.5	RAIRS	[78]	—	—
		467	2104	0.5	RAIRS	[79]	—	—
			2093	0.07	RAIRS	[80]	—	—
			2095	0.1	RAIRS	[81]	—	—
			2100	0.25	RAIRS	[82]	—	—
	Bridge	380	1850	0.24	EELS	[50]	372	1880
		376		0.5	RAIRS	[78]	—	—
			1855	0.5	RAIRS	[79]	—	—
			1858	0.07	RAIRS	[80]	—	—
	Hollow		1810	0.5	RAIRS	[82]	352	1793
			1736	0.51	RAIRS	[83]	—	—

on the trends in binding energy or geometrical structure of the CO molecule on a metallic surface [8, 10]. The importance of the interplay between the geometric and the electronic structure in the understanding of CO adsorption was stressed by Föhlisch *et al* [84]. In our analysis we essentially follow the ideas expressed in [85–87].

How is CO adsorbed on the TM surface? It is generally assumed that a major part of the CO–metal interaction can be explained in terms of frontier orbitals (the highest occupied molecular orbital (HOMO) and the lowest occupied molecular orbital (LUMO) orbitals). The Blyholder model is based on the donation from the occupied CO-5σ states into empty surface orbitals and the back-donation from occupied surface orbitals to the CO-2$\pi^\star$ orbitals [1].

At this point we can divide the literature into three groups. To the first belong those that agree completely with the Blyholder model [1, 88, 89]. The second group consists of those that agree with Blyholder (in principle), but point out that the Blyholder model ignores the contribution to the bonding from the 4σ and 1π orbitals. Some consider the model not only oversimplified but propose another $2\pi^\star$ resonance model, like Gumhalter *et al* [90]. Finally, to the third group belong those that disagree with the Blyholder model and claim that there is no back-donation to the $2\pi^\star$ orbital [91].

Although in the experimental study of Nilsson *et al* [92], the authors emphasize that an atom-specific look at the CO adsorption could provide an insight into the surface chemical bond, we have projected the DOS onto the molecular CO orbitals. The density of states projected onto 1π, $2\pi^\star$, 5σ and 4σ molecular orbitals (PDOS) of a CO molecule in top, bridge and hollow sites and a CO molecule far above ($\sim$4 Å) the surface is depicted in figure 10. The weakly bonded CO molecules on the Au(111) surface already show the general interaction trends. The corresponding analysis of the orbitals of a CO molecule on Pt(111) can also be found in the paper by Kresse *et al* [85].

There is no principal difference between the Au and Pt DOS. As the CO molecule approaches the surface the localized CO orbitals, 3σ (not shown) and 4σ, are shifted to lower energies, depending on the coordination between $\sim$1 and 3 eV. Since they are fully occupied they play only a minor role in the interaction with the metal, characterized as Pauli repulsion. On the other hand, the 5σ, 1π and $2\pi^\star$ peaks broaden and dominate the interaction. Again, the broadening and the shift of the peaks increase with coordination: the higher the coordination the greater the shift and the broadening. This behaviour is more visible for the $5\tilde{\sigma}$ than for the $2\tilde{\pi}^\star$ peak. The position of the $5\tilde{\sigma}$ band peak is almost always lower than the $1\tilde{\pi}$ peak, which is shifted by $\sim$1–3 eV. The $5\tilde{\sigma}$ band is higher in energy only for on-top adsorption of CO on the Ag(111) surface, which is partially related to the weak interaction. A typical shift for the 5σ peak is 3–4 eV, depending on the metal–CO bond strength. Finally, the $2\pi^\star$ band also broadens with increasing coordination and is therefore partially shifted below the Fermi level ($E_{\mathrm{Fermi}} = 0$ eV) as shown in figure 10.

The detailed interaction picture on different sites depends on the symmetry of the surface and adsorbate orbitals. For the top site the major orbital interaction (due to symmetry) is 5σ (CO)–d_{z^2} (metal), whereas for the higher coordinated sites the 1π and $2\pi^\star$ CO molecular orbitals are more important, interacting with the d_{xz} (resp. d_{yz}) and in-plane ($d_{x^2-y^2}$, d_{xy}) orbitals of the metal atoms. The 5σ orbital of the CO orbital adsorbed on top hybridizes with the d_{z^2} states of the metallic substrate and shifts to lower energies. The d_{z^2} states broaden and split into a $5\sigma - d_{z^2}$ bonding contribution far below the Fermi-level ($\sim$7.5 eV) and $5\sigma - d_{z^2}$ anti-bonding contributions located above the bonding peak and partly even above the Fermi level. This interaction would be repulsive (Pauli-like) if the $5\sigma - d_{z^2}$ were not pushed partly above the Fermi level. A 5σ depletion (donation from CO to metal) is in accordance with the Blyholder argument of donation of electrons from the adsorbate to the surface [1]. The interaction between the 5σ orbitals and the metal s band is attractive, but depends on the amount of electrons accumulated in the newly created molecular orbitals of the CO–metal system. If we consider a depletion of the 5σ orbital, then the interaction with the metallic s band becomes more attractive.

The interaction between the 1π (resp. $2\pi^\star$) orbitals and the substrate is more complex [84]: we can distinguish four contributions:

(i) The main part of the 1π CO orbital is located at energies around ~ -6 eV.

(ii) During adsorption the peak broadens at the higher energy end up to the Fermi level. This broad state is usually called the $d_{\tilde{\pi}}$ orbital. All the interactions with the 1π orbital are located below the Fermi level and have repulsive character [93].

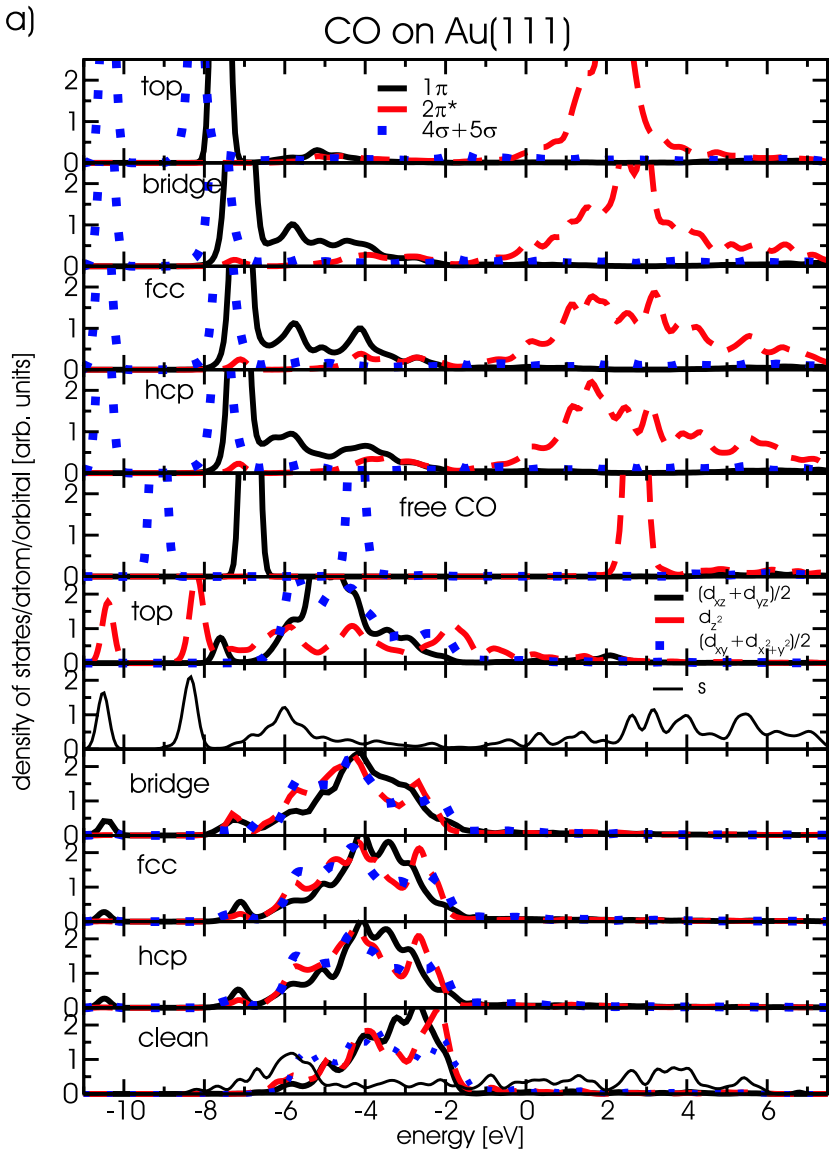

Figure 10. The projected electronic densities of states (PDOS) for the CO molecule adsorbed in top, bridge, fcc and hcp hollow sites of the Au (a) and Pt (b) surfaces. While the upper five panels describe the PDOS for various molecular orbitals of the CO molecule, the lower six panels show the PDOS for the substrate atom(s) interacting most with the molecule. The panels labelled 'free CO' and 'clean' describe the noninteracting case for comparison (a molecule 4 Å above the surface). The DOS is smoothed by a Gaussian function with a width of 0.2 eV and the Fermi level is located at 0 eV.

(This figure is in colour only in the electronic version)

(iii) Furthermore, in the same energy region is a contribution from a partially occupied $2\pi^\star$ orbital which increases with coordination and decreases with d-band filling (see figure 10). This contribution develops into a broad peak for Pt.

(iv) Finally, at higher energies (∼3 eV) the anti-bonding $2\pi^\star$–$d_{yz}(d_{xz})$ hybridized orbital is visible.

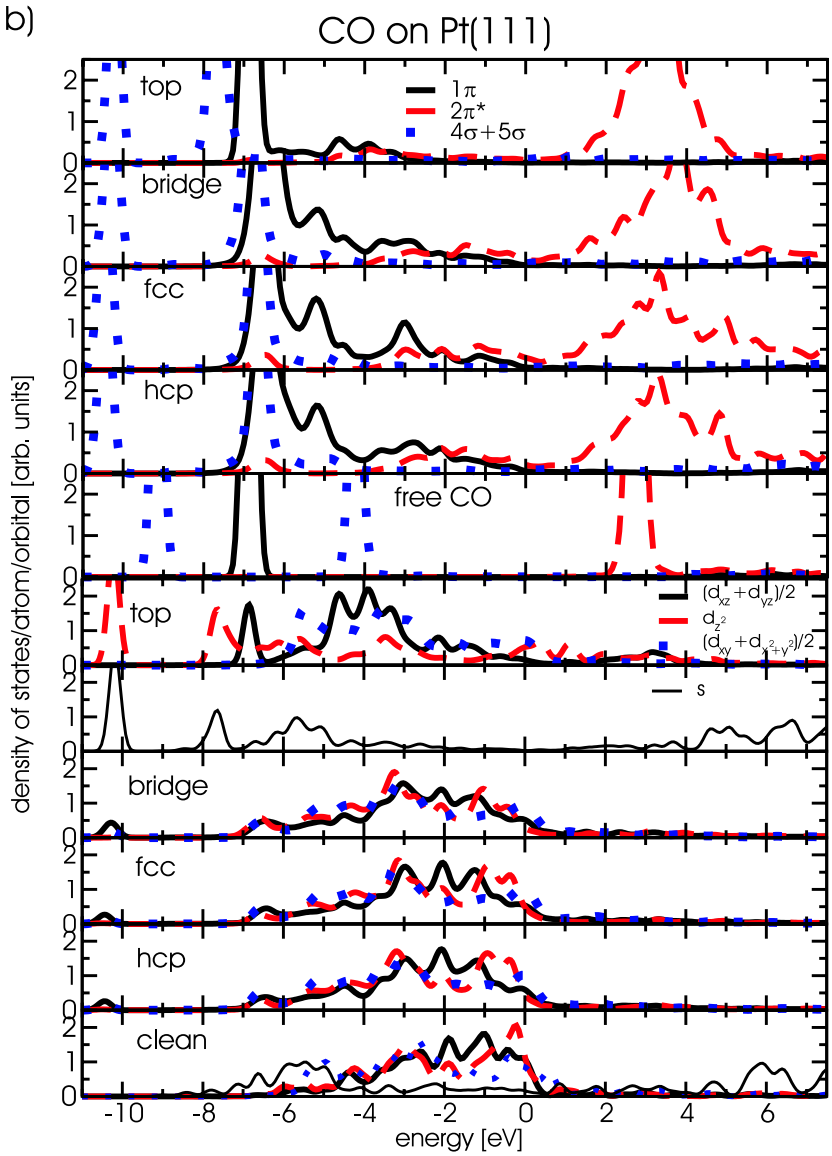

Figure 10. (Continued.)

The latter two contributions can be characterized by the fractional occupation of the $2\tilde{\pi}^{\star}$ orbital, compiled in table 4. At this point one should remark that our representation of the DOS projected onto molecular orbitals is subject to small inaccuracies, not in position but in amplitude, arriving from the projection of the plane-wave components. There exists a tiny hybridization between the molecular $1\tilde{\pi}$ and $2\tilde{\pi}^{\star}$ orbitals. Therefore the calculated DOS is slightly overestimated at the position of the $2\tilde{\pi}^{\star}$ for the $1\tilde{\pi}$ and at the position of the $1\tilde{\pi}$ for $2\tilde{\pi}^{\star}$. This must be considered when calculating the occupation of the $2\tilde{\pi}^{\star}$ orbital.

The occupation of the $2\tilde{\pi}^{\star}$ orbital increases with coordination but decreases with d-band filling and also from the 3d to the 4d and 5d elements. We can further correlate the site preference between the two competitive (fcc and hcp) hollow sites to the occupation of the

Table 4. Fractional occupation of the $2\tilde{\pi}^\star$ orbital for the CO molecule in top, bridge, fcc and hcp sites on the close-packed TM surfaces in %.

	Occupation of $2\tilde{\pi}^\star$									
Site	Co	Ni	Cu	Ru	Rh	Pd	Ag	Ir	Pt	Au
Top	16.0	11.5	8.1	11.4	10.8	8.8	5.3	11.4	10.0	6.0
Bridge	19.5	14.5	11.1	12.5	11.4	10.5	7.0	11.1	10.1	7.4
fcc	29.9	22.1	16.3	18.5	18.5	18.1	11.7	20.5	19.8	15.0
hcp	29.7	21.6	16.1	19.9	19.5	18.2	11.5	21.4	19.7	14.4

$2\tilde{\pi}^\star$ orbital. As the occupation of the orbital for the fcc site compared to hcp site increases, the site preference changes from the hcp to the fcc hollow sites. This effect is probably due to a better interaction with the metal atom in the second layer below the hcp site for metals with smaller lattice constants.

4.5. Charge density redistribution

In this section, we illustrate the ideas derived in the previous section from analysis of the DOS by analysing the charge density and the difference in the charge density for the molecular orbitals of the CO molecule adsorbed on top on the Au(111) surface, as shown in figure 11. At first we show the 4σ, 5σ and 1π orbital-decomposed charge density of the free CO molecule (panels (a)–(c)). We can see the accumulation of the charge density for the 4σ and 1π orbitals around the oxygen atom and for the 3σ (not shown) and 5σ orbitals on the carbon atom. Figures 11(d)–(f) illustrate what happens to these orbitals after the CO molecule is chemisorbed on top on the Au(111) surface. Within the 4σ orbital charge density moves from the C–O bond and from above the oxygen atom to the region below the carbon (figure 11(d)). Figure 11(e) shows the redistribution of charge in the 5σ molecular orbital: charge is transferred from the side located closer to the metal to the opposite side of the carbon and oxygen atoms. This charge transfer is in line with the experimental observation of a lone pair localized on the oxygen atom, as reported in [92]. There is only a little transfer of charge density from the oxygen orbitals with p_x/p_y character into the metal–carbon bond ($1\tilde{\pi}$). This redistribution could be related to the slight inaccuracy of the orthogonalization of $1\tilde{\pi}$ and $2\tilde{\pi}^\star$ orbitals.

The newly formed hybrid states, either by broadening of the 1π orbital ($d_{\tilde{\pi}}$) or by occupation of $2\pi^\star$ orbitals, are shown in panels (g) and (h). The $d_{\tilde{\pi}}$ orbital shows a charge transfer from the d orbitals towards the π-like molecular orbitals. We can even spot a small depletion of charge at the metal atom which is only a second nearest neighbour of the CO, charge which is attracted towards the metal atom interacting with the CO molecule. Furthermore, $2\tilde{\pi}^\star$ states become occupied as can be seen in figure 11(h). In panel (i), we present the total charge density difference of all states, i.e. the sum of all mentioned charge density redistributions.

Summarizing, we can say that there is a depletion of charge in the substrate out-of-plane d orbitals and an accumulation of charge density in the in-plane d orbitals of the substrate. The charge density on CO is redistributed and additionally some charge is transferred into $2\pi^\star$-like orbitals, which weakens the C–O bond. The establishment of the M–CO bond is reflected by the accumulation of charge between the bonding species.

5. Improving site preference

As previously mentioned the calculations for Cu, Rh and Pt surfaces predict a wrong site preference for CO adsorption and the adsorption energies for different adsorption sites on

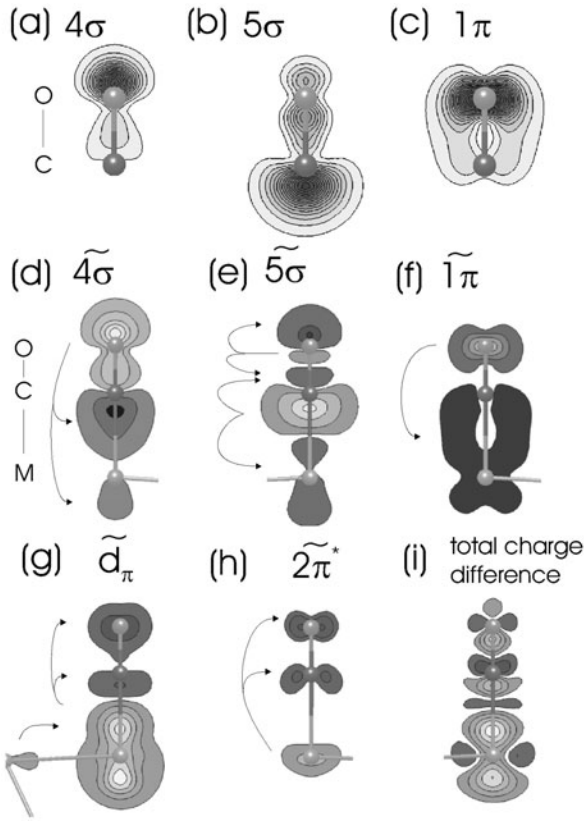

Figure 11. Charge density of (a) 4σ, (b) 5σ and (c) 1π CO orbitals for the free molecule and the difference ($\Delta\rho = \rho_{\mathrm{CO+Au(111)}} - \rho_{\mathrm{Au(111)}} - \rho_{\mathrm{CO}}$) after adsorption in the top site of the Au(111) surface (figures (d), (e) and (f)). Figures (g) and (h) show the change in the metal charge density due to CO adsorption in the energy interval (-5.9, -1.0) and just below Fermi level (-0.2,E_{F}). The total charge density difference due to adsorption is shown in figure (i). Dark regions: charge accumulation; light regions: charge depletion.

Co, Ag and Au are almost degenerate, so that small changes in the set-up (k points and neglect of surface relaxation) can alter the site preference. Can harder pseudopotentials (lower r_{cut} in the pseudopotential generation) or different GGA approaches influence the site preference? In order to shed light onto this question we repeated our calculations performed with the PW91 exchange–correlation functional and cut-off energy $E_{\mathrm{cut}} = 450$ eV with a harder pseudopotential which requires a higher $E_{\mathrm{cut}} = 700$ eV and used two different GGA functionals: PW91 and RPBE. The use of RPBE is known to result in lower adsorption energies for CO, improving the agreement with experiment in most cases [17] with an almost unchanged geometrical structure. The results for RPBE with $E_{\mathrm{cut}} = 700$ eV (calculated at the optimized PW91 geometry) are presented in figure 12.

Switching to the RPBE GGA changes the energetics drastically by $\sim$0.3 eV and the values agree well with experiment for strong chemisorption. On the other hand, the deviation from the experimentally determined adsorption energy increases for weak bonding. For Ag and Au, the RPBE even predicts CO adsorption to be endothermic. Furthermore, the RPBE functional removes the degeneracy of the adsorption sites for Co(0001) and Ag(111) surfaces and on-top sites become clearly favoured. The favoured sites for CO on Rh, Pt and Cu still contradict

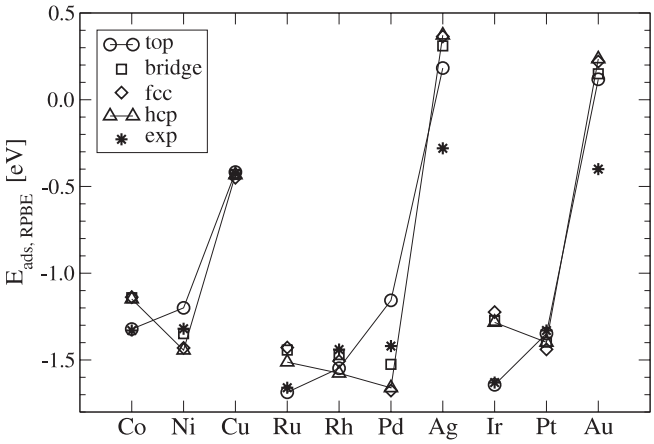

Figure 12. CO adsorption energies on TM surfaces for the RPBE exchange–correlation functional and energy cut-off 700 eV. Experimental CO heats of desorption are labelled by stars (see table 1), while calculated adsorption energies for top sites are shown by triangles, for bridges by squares, for fcc hollows by diamonds and for hcp sites by circles.

the experimental findings. However, in all these cases the corrugation of the potential energy surface is very small compared to metals where CO satisfies the experimental site preference (e.g. Ir and Pd [3]). This also indicates that it is harder for the CO molecule to find the optimal adsorption site on these metals.

To make sure that this large change in E_{ads} is not the effect of the E_{cut} (larger basis set), but of the different functional, we have recalculated all systems with a harder PW91 pseudopotential, which also requires an energy cut-off of $E_{\mathrm{cut}} = 700$ eV. Besides a small reduction of the adsorption energies (weaker bonding) by about 50 meV the results are identical to those obtained for $E_{\mathrm{cut}} = 450$ eV.

Summarizing, harder pseudopotentials for C and O lead to a slight decrease of the adsorption energies. The RPBE exchange–correlation functional reduces the adsorption energies by $\sim$0.3 eV and improves the differences in adsorption energies for different adsorption sites. However, the site preference remains the same as for the PW91 functional.

6. Discussion

In this section, we discuss trends which can be deduced from our results for CO adsorption on close-packed transition and noble metal surfaces.

6.1. Correlations between adsorbate geometry, frequency and adsorption energy

A strong correlation exists between the C–O bond length and the stretching frequency of the CO molecule $\nu_{\mathrm{C-O}}$. During adsorption the $2\pi^\star$ orbital is partially populated and the C–O bond is weakened. This filling increases from the right to the left in the periodic table and with increasing coordination of the adsorption site and hence the CO bond length increases. A weaker and therefore longer C–O bond implies stronger CO–metal bonding and results in lower C–O stretching frequencies. The dependence of $d_{\mathrm{C-O}}$ on the coordination is smallest for the 3d and largest for the 4d metals, as can be seen in figure 7. The trend goes as follows: the higher the reactivity of the surface, the stronger the bonding and population of $2\pi^\star$-derived orbitals, resulting in a more elongated C–O bond length and a lower stretching frequency.

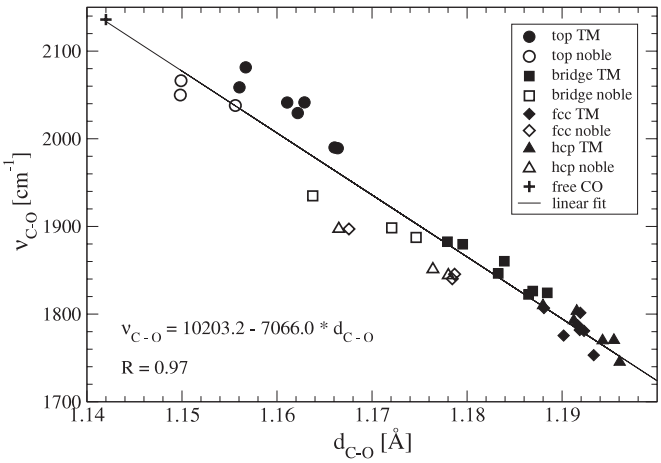

Figure 13. Correlation between the calculated CO bond length (d_{C-O}) and the C–O stretching frequency (ν_{C-O}) for all high-symmetry adsorption sites.

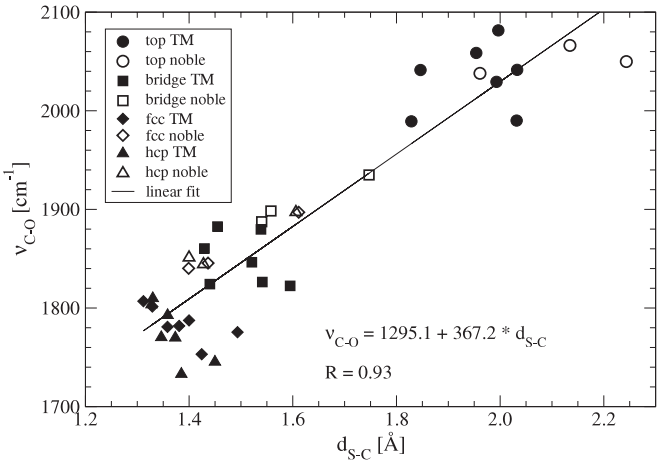

Figure 14. Correlation between the calculated S–C distance (d_{S-C}) and the C–O stretching frequency (ν_{C-O}) for all high-symmetry adsorption sites.

In figure 13 the CO stretching frequency is plotted versus the molecular bond length, exhibiting a linear relationship between these two properties which is almost independent of the coordination of the CO molecule. The linear regression fit is characterized by a correlation coefficient of $R = 0.97$.

As expected, pronounced stretching of the CO bond (reflecting a stronger adsorbate–substrate interaction) is accompanied by a decrease of the adsorption height. In figure 14 we present this linear relationship between the vibrational frequency ν_{CO} and the surface–carbon distance. Remarkably, a trend established by noble metals alone would be characterized by a much bigger correlation coefficient of $R = 0.98$ (fit not shown) compared to the correlation coefficient of $R = 0.93$ for the complete dataset.

Although we cannot directly relate the height of the molecule on the surface to the adsorption energy it serves as a rough estimate of the metal–adsorbate interaction. As a

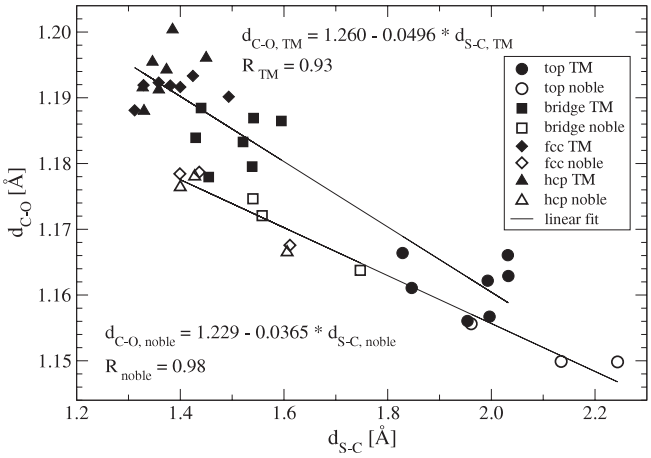

Figure 15. Correlation between the calculated CO bond length (d_{C-O}) and the S–C distance (d_{S-C}) for all high-symmetry on-surface sites.

consequence of these two linear relationships (d_{C-O} to ν_{CO} and d_{S-C} to d_{C-O}) a similar correlation exists between the d_{S-C} and d_{C-O} (figure 15). Again, we have divided our dataset into two groups: noble and transition metals and we provide separately a linear fit for each group of our set. Again, the correlation coefficient is higher for noble ($R_{noble} = 0.98$) than for transition metals ($R_{TM} = 0.93$).

The above-mentioned linear relationships have an important consequence: if we know one of the four measured properties (ν_{C-O}, d_{C-O}, d_{S-C} or d_{M-C}) we can easily estimate all the other linearly related properties.

6.2. Correlation between the electronic properties of the substrate and adsorption energy

As already mentioned above, one of the most widely discussed models for molecular adsorption on TM surfaces is the d-band model of Hammer and Nørskov [8, 9] relating the chemisorption energy to the position of the metallic d band relative to the molecular orbitals of the adsorbate and to the coupling matrix elements and overlap integrals between the metal d states and adsorbate states. In a simplified form of the argument, the adsorption energy is related to the d-band position only. This simplified d-band model has recently been examined by Lu *et al* [94] for the adsorption of CO, H_2 and ethylene. This analysis led the authors to a critique of the d-band model and of DFT calculations of adsorption energies in general. For CO it was pointed out that the reduction of the adsorption energies with increasing distance of the d-band centre from the Fermi energy follows qualitatively the predicted trend, but quantitatively the theoretically predicted dependence is much stronger than what is observed experimentally.

In figure 16 we present calculated CO adsorption energies (PW91) with respect to the d-band centres taken from figure 4. We can clearly establish a linear relationship between the position of the d-band centre and the adsorption energy for CO adsorption on noble metals. On the other hand, the values for the transition metals show a large scatter. Hence what really determines the trend are the noble metals. It does not mean that there is no relation between the adsorption energy and the d-band centre, but it must be corrected for the variation of the coupling matrix elements between different metals, as in the original argument of Hammer and Nørskov [8].

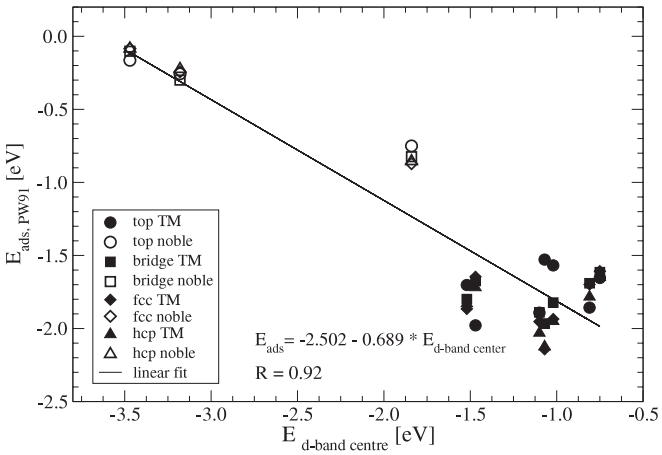

Figure 16. Correlation between the calculated position of the d-band centre (where at least 9.5 electrons are accumulated, see figure 4) for all high-symmetry on-surface sites. Empty symbols are for noble metals and full symbols are for transition metals.

6.3. Site preference—limitation of DFT

As a by-product of this study the performance of the PW91 functional with different E_{cut} (harder potential) and the RPBE functional (well suited for CO and NO adsorption) could be tested on a large number of systems.

A calculation with a harder pseudopotential for the same exchange–correlation functional (PW91) leads to small changes in the heat of adsorption, which is closer to the experimental value for TM but further for noble metals. The site preference does not depend on the basis set for the PW91 exchange–correlation functional.

The most important difference between the PW91 and RPBE functionals with a more accurate pseudopotential ($E_{\mathrm{cut}} = 700$ eV) is in the absolute value of the adsorption energy $\Delta E_{\mathrm{ads}} \sim 0.3$ eV. Moreover, the difference in the adsorption energy between the previously almost degenerate top and hollow adsorption sites is increased (Co, Ag, Au). However, all these changes do not correct the prediction of a wrong adsorption site for Cu, Rh and Pt.

Hence the question 'Why does DFT fail in predicting the right adsorption site as well as energy?' arises. In the past, it has been proposed that a relativistic treatment of TM could solve the problem [95–97]. However, the results presented to support this suggestion are not really convincing, being based on rather thin slabs. Also we note that the work function of the TM is well described and the electronic structure calculations are in good agreement with spectroscopic results. A more promising approach starts from the observation that $2\pi^\star$ back-donation is the most important contribution to the adsorbate–substrate bond. It is well known that DFT calculations tend to underestimate the HOMO–LUMO gap in CO, facilitating back-donation. Very recently, Kresse *et al* [85] have used a LDA + U approach, leading to an increased HOMO–LUMO splitting due to an additional on-site Coulomb repulsion. It was shown that, with an increasing HOMO–LUMO gap on Pt(111), $2\pi^\star$ back-donation favouring hollow adsorption is reduced and the site preference switches to the correct top site.

Another way to improve the HOMO–LUMO gap is to use hybrid functionals mixing DFT-exchange with exact (Hartree–Fock) exchange: for gas-phase CO the PW91 functional predicts a HOMO–LUMO gap of 6.8 eV, whereas the B3LYP hybrid functionals predict a splitting of 10.1 eV. However, B3LYP calculations can, at the moment, only be performed using localized basis sets and small clusters. Very recently Gil *et al* [98] have performed a series of cluster

calculations for CO on Pt(111) using both PW91 and B3LYP functionals and slab calculations using PW91. The conclusion is that the B3LYP functional reduces the overestimation of the stability of the hollow site compared to PW91 for a given cluster size. However, the results also show a pronounced cluster-size dependence: for small clusters the preference for the hollow site is more pronounced than for larger clusters (the largest cluster considered in this study is Pt_{19}). For a comparison of cluster and slab calculations it is concluded that a slab calculation, if performed with a B3LYP functional, should favour top adsorption, in agreement with experiment.

Current work is devoted to extension of the LDA + U approach to other metals and to the investigation of the influence of meta-GGA functionals (incorporating a dependence on the kinetic energy density).

7. Conclusions

The adsorption behaviour of the CO molecule on the surfaces of close-packed late TM, namely Co, Ni, Cu, Ru, Rh, Pd, Ag, Ir, Pt and Au has been analysed using *ab initio* DFT methods. To rationalize the trends in CO adsorption we performed investigations of the geometric structure (metal surface–C and C–O bond lengths), the electronic structure (projected DOS, charge flow analysis) and the vibrational properties (ν_{C-O} and ν_{M-CO}). In addition, we examined the influence of different GGAs (PW91, RPBE) on the CO site preference and adsorption energies.

We demonstrate that the current DFT slightly overestimates substrate lattice constants (by 1–2%) and underestimates the work function (by about 0.3 eV). We compared our calculated values for the geometric structure of the adsorbate–substrate complex with experimental data and we find them in very good agreement. Furthermore, the C–O and M–CO stretching frequencies agree well with experiments. We illustrate the detailed interaction picture of the CO molecules for different adsorption sites on TM surfaces by means of the density of states projected onto molecular CO orbitals and the change of the charge density due to adsorption.

The present density functionals overestimate the adsorption energy for sites with high metal coordination compared to sites with low metal coordination. Moreover, the underestimated energy difference between HOMO (5σ) and LUMO ($2\pi^\star$) orbitals contributes to the CO over-binding. DFT fails in predicting the site preference for CO on the Cu (by $\geqslant$30 meV), Rh (by $\geqslant$30 meV) and Pt (by $\geqslant$90 meV) close-packed metal surfaces at 0.25 ML coverage.

Different GGA functionals reduce these discrepancies, but neither harder potentials for CO nor different GGA functionals correct the results for CO adsorption on these substrates. One should also point out that the adsorption energies calculated using RPBE exchange–correlation functionals give results which are much closer to the experimental values for TM surfaces but predict CO adsorption to be endothermic on the noble metals (Ag and Au).

Recent results have shown that a correct site preference can be achieved by correcting the HOMO–LUMO gap using techniques beyond DFT. This is after all not entirely surprising, since the analysis demonstrates the importance of the $2\pi^\star$ back-donation effects, i.e. electron transfer to excited states of the free molecule.

References

[1] Blyholder G 1964 *J. Phys. Chem.* **68** 2772
[2] Bagus P S, Nelin C J and Bauschlicher C W 1983 *Phys. Rev.* B **28** 5423
[3] Over H 2001 *Prog. Surf. Sci.* **58** 249
[4] Sung S and Hoffmann R 1985 *J. Am. Chem. Soc.* **107** 578
[5] Feibelman P, Hammer B, Nørskov J K, Wagner F, Scheffler M and Stumpf R 2001 *J. Phys. Chem.* B **108** 4018
[6] Ying S C, Smith J R and Kohn W 1975 *Phys. Rev.* B **11** 1483

[7] Andreoni W and Varma C M 1981 *Phys. Rev.* B **23** 437
[8] Hammer B and Nørskov J K 2000 *Adv. Catal.* **45** 71
[9] Nørskov J K 1990 *Rep. Prog. Phys.* **53** 1253
[10] Ishi S, Ohno Y and Viswanathan B 1985 *Surf. Sci.* **161** 349
[11] http://cms.mpi.univie.ac.at/vasp/
[12] Kresse G and Furthmüller J 1996 *Phys. Rev.* B **54** 11169
[13] Blöchl P 1994 *Phys. Rev.* B **50** 17953
[14] Kresse G and Joubert D 1999 *Phys. Rev.* B **59** 1758
[15] Perdew J P and Zunger A 1981 *Phys. Rev.* B **23** 5048
[16] Perdew J P, Chevary J A, Vosko S H, Jackson K A, Pederson M R, Singh D J and Fiolhais C 1992 *Phys. Rev.* B **46** 6671
[17] Hammer B, Hansen L B and Nørskov J K 1999 *Phys. Rev.* B **59** 7413
[18] Mantz A W, Watson J K G, Rao K N, Albritton D L, Schmeltekope A L and Zare R N 1971 *J. Mol. Spectrosc.* **39** 180
[19] Cox J D, Wangman D D and Medvedev V A 1984 *CODATA Key Values for Thermodynamics* (New York: Hemisphere)
[20] *Strukturdaten der Elemente und Intermetallischer Phasen* 1971 (*Landolt–Börnstein Neue Serie* Group III) (Berlin: Springer)
[21] Wu M W and Metiu H 2000 *J. Chem. Phys.* **113** 1177
[22] Mavrikakis M, Hammer B and Nørskov J K 1998 *Phys. Rev. Lett.* **81** 2819
[23] Michaelson H B 1977 *J. Appl. Phys.* **48** 4729
[24] Himpsel F J, Christmann K, Heimann P, Eastmann D E and Feibelmann P J 1982 *Surf. Sci.* **115** L159
[25] Böttcher A and Niehus H 1999 *Phys. Rev.* B **60** 14396
[26] Hendrickx H A C M 1988 *PhD Thesis* Rijksuniversiteit Leiden, The Netherlands
[27] Fischer R, Schuppler S, Fischer N, Fauster T and Steineman W 1993 *Phys. Rev. Lett.* **70** 654
[28] Nieuwenhuys B E 1973 *Surf. Sci.* **34** 317
[29] Hammer B and Nørskov J K 1995 *Surf. Sci.* **343** 211
[30] Hammer B, Morikawa Y and Nørskov J K 1996 *Phys. Rev. Lett.* **76** 2141
[31] Somorjai G 1979 *Surf. Sci.* **89** 496
[32] Papp H 1983 *Surf. Sci.* **129** 205
[33] Lahtinen J, Vaari J and Kauraala K 1988 *Surf. Sci.* **418** 502
[34] Stuckless J T, Al-Sarraf N, Wartnaby C and King D A 1993 *J. Chem. Phys.* **203** 2202
[35] Froitzheim H and Koehler U 1987 *Surf. Sci.* **188** 70
[36] Miller J B, Siddiqui H R, Gates S M, Russell J N Jr, Yates J T Jr, Tully J C and Cardillo M J 1987 *J. Chem. Phys.* **87** 6725
[37] Vollmer S, Witte G and Woell C 2001 *Catal. Lett.* **77** 97
[38] Kirstein W, Krüeger B and Thieme F 1986 *Surf. Sci.* **176** 505
[39] Kessler J and Thieme F 1977 *Surf. Sci.* **67** 405
[40] Pfnür H and Menzel D 1983 *J. Chem. Phys.* **79** 4613
[41] Smedh H A B, Borg M, Nyholm R and Andersen J N 2001 *Surf. Sci.* **491** 115
[42] Thiel P A, Wiliams E D and Yates J T 1979 *Surf. Sci.* **84** 54
[43] Wei D H, Skelton D C and Kevan S D 1997 *Surf. Sci.* **381** 49
[44] Perlinz K A, Curtiss T J and Sibener S J 1991 *J. Chem. Phys.* **95** 6972
[45] Szanyi J, Kuhn W K and Goodman D W 1993 *J. Vac. Sci. Technol.* A **11** 1969
[46] Guo X and Yates J T Jr 1989 *J. Chem. Phys.* **90** 6761
[47] McElhiney G, Papp H and Pritchard J 1976 *Surf. Sci.* **54** 617
[48] Sushchikh M, Lauterbach J and Weinberg W H 1997 *J. Vac. Sci. Technol.* A **15** 1630
[49] Comrie C M and Weinberg W H 1976 *J. Chem. Phys.* **64** 250
[50] Steininger H, Lehwald S and Ibach H 1982 *Surf. Sci.* **123** 264
[51] Seebauer E G, Kong A C F and Schmidt L D 1987 *J. Vac. Sci. Technol.* **5** 464
[52] Ertl G, Neumann M and Streit K M 1977 *Surf. Sci.* **64** 393
[53] Elliott G S and Miller D R 1984 *Proc. 14th Int. Symp. on Rarefied Gas Dynamics* (Tokyo: University of Tokyo Press) pp 349–58
Elliott G S and Miller D R 2003 personal communication
[54] Westerlund L, Jönsson L and Andersson S 1988 *Surf. Sci.* **199** 109
[55] Lahtinen J, Vaari J, Kauraala K, Soares E A and Van Hove M A 2000 *Surf. Sci.* **448** 269
[56] Eichler A 2003 *Surf. Sci.* **526** 332
[57] Moler E J, Kellar S A, Huff W R A and Hussain Z 1996 *Phys. Rev.* B **54** 10862

[58] Over H, Moritz W and Ertl G 1993 *Phys. Rev. Lett.* **70** 315
[59] Gierer M, Barbieri A, Van Hove M A and Somorjai G A 1997 *Surf. Sci.* **391** 176
[60] Giessel T, Schaff O, Hirschmugl C J, Fernandez V, Schindler K M, Theobald A, Bao S, Lindsay R, Berndt W, Bradshaw A M, Baddeley C, Lee A F, Lambert R M and Woodruff D P 1998 *Surf. Sci.* **406** 90
[61] Ohtani H, Van Hove M A and Somorjai G A 1987 *Surf. Sci.* **187** 372
[62] Blackman G S, Xu M L, Ogletree D F, Van Hove M A and Somorjai G A 1988 *Surf. Sci.* **61** 2353
[63] Beitel G A, Laskov A, Oosterbeek H and Kuipers W W 1996 *J. Phys. Chem.* **100** 12494
[64] Hirschmugl C J, Williams G P, Hoffmann F M and Chabal Y J 1990 *J. Electron Spectrosc. Relat. Phenom.* **54/55** 109
[65] Raval R, Parker S F, Pemble M E, Hollins P, Pritchard J and Chester M A 1988 *Surf. Sci.* **203** 353
[66] Eve J K and McCash E M 1999 *Chem. Phys. Lett.* **313** 575
[67] Thomas G E and Weinberg W H 1979 *J. Chem. Phys.* **70** 954
[68] Jacob P and Person B N J 1997 *Phys. Rev. Lett.* **78** 3503
[69] He P, Dietrich H and Jacobi K 1996 *Surf. Sci.* **345** 241
[70] Dubois L H and Somorjai G A 1979 *Surf. Sci.* **91** 514
[71] Smedh M, Beutler A, Ramsvik T, Nyholm R, Borg M, Andersen J N, Duschek R, Sock M, Netzer F P and Ramsey M G 2001 *Surf. Sci.* **491** 99
[72] Bradshaw A M and Hoffmann F M 1978 *Surf. Sci.* **72** 513
[73] Surnev S, Sock M, Ramsey M G, Netzer F P, Wiklund M, Borg M and Andersen J N 2000 *Surf. Sci.* **470** 171
[74] Hansen W, Bertolo M and Jacobi K 1991 *Surf. Sci.* **253** 1
[75] Schick M, Lauterbach J and Weinberg W H 1996 *J. Vac. Sci. Technol.* A **14** 1448
[76] Lauterbach J, Boyle R W, Schick M, Mitchell W J, Meng B and Weinberg W H 1996 *Surf. Sci.* **350** 32
[77] Kung K Y, Chen P, Wei F, Shen Y R and Somorjai G A 2000 *Surf. Sci.* **463** L627
[78] Surman M, Hagans P L, Wilson N E, Baily C J and Russell A E 2002 *Surf. Sci.* **511** L303
[79] Schweizer E, Persson B N J, Tüshaus M, Hoge D and Bradshaw A M 1989 *Surf. Sci.* **213** 49
[80] Nekrylova J V and Harrison I 1996 *Chem. Phys.* **205** 37
[81] Yoshinobu J and Kawai M 1996 *Surf. Sci.* **363** 105
[82] Heyden B E and Bradshaw A M 1983 *Surf. Sci.* **125** 787
[83] Nekrylova J V, French C, Artsyukhovich A N, Ukraintsev V A and Harrison I 1993 *Surf. Sci. Lett.* **295** L987
[84] Föhlisch A, Nyberg M, Hasselström J, Karis O, Pettersson L G M and Nilsson A 2000 *Phys. Rev. Lett.* **85** 3309
[85] Kresse G, Gil A and Sautet P 2003 *Phys. Rev.* B **68** 073401
[86] Bagus P S and Pacchioni G 1972 *Surf. Sci.* **278** 427
[87] Hoffmann R 1988 *Rev. Mod. Phys.* **60** 601
[88] Illas F, Zurita S, Rubio J and Márquez A M 1997 *Surf. Sci.* **376** 279
[89] Aizawa H and Tsuneyuki S 1998 *Surf. Sci.* **399** L364
[90] Gumhalter B, Wandelt K and Avouris P 1988 *Phys. Rev.* B **37** 8048
[91] Ohnishi S and Watari N 1994 *Phys. Rev.* B **49** 14619
[92] Nilsson A, Weinelt M, Wiell T, Bennich P, Karis O and Wassdahl N 1997 *Phys. Rev. Lett.* **78** 2847
[93] Hu P, King D A, Lee M-H and Payne M C 1995 *Chem. Phys. Lett.* **246** 73
[94] Lu C, Lee I C, Masel R I, Wieckowski A and Rice C 2002 *J. Phys. Chem.* A **106** 3084
[95] Geschke D, Baştuğ T, Jacob T, Fritzsche S, Sepp W-D, Fricke B, Varga S and Anton J 2001 *Phys. Rev.* B **64** 235411
[96] Grinberg I, Yourdshahyan Y and Rappe A M 2002 *J. Chem. Phys.* **117** 2264
[97] Olsen R A, Philipsen P H T and Baerends E J 2003 *J. Chem. Phys.* **119** 4522
[98] Gil A, Clotet A, Ricart J M, Kresse G, García-Hernández M, Rösch N and Sautet P 2003 *Surf. Sci.* **530** 71